2001

Measurement of the Gluon Parton Distribution Function at Small x with Neutrino Telescopes

Gabriele U. Varieschi
Loyola Marymount University, gvarieschi@lmu.edu

Recommended Citation

G. Gelmini, P. Gondolo and G. Varieschi, "**Measurement of the gluon partonic distribution function at small x with neutrino telescopes**," Phys. Rev. D 63, 036006, 2001.

Measurement of the gluon parton distribution function at small x with neutrino telescopes

Graciela Gelmini*
Department of Physics and Astronomy, UCLA (University of California, Los Angeles), 405 Hilgard Avenue, Los Angeles, California 90095

Paolo Gondolo†
Max-Planck-Institut für Physik, Werner-Heisenberg-Institut, Föhringer Ring 6, 80805 München, Germany

Gabriele Varieschi‡
Department of Physics and Astronomy, UCLA (University of California, Los Angeles), 405 Hilgard Avenue, Los Angeles, California 90095
and Department of Physics, Loyola Marymount University, 7900 Loyola Boulevard, Los Angeles, California 90045
(Received 31 March 2000; revised manuscript received 4 October 2000; published 10 January 2001)

We analyze the possibility that neutrino telescopes may provide an experimental determination of the slope λ of the gluon distribution in the proton at momentum fractions x smaller than the accelerator reach. The method is based on a linear relation between λ and the spectral index (slope) of the down-going atmospheric muon flux above 100 TeV, for which there is no background. Considering the uncertainties in the charm production cross section and in the cosmic ray composition, we estimate the error on the measurement of λ through this method, excluding the experimental error of the telescopes, to be ± 0.2.

DOI: 10.1103/PhysRevD.63.036006 PACS number(s): 96.40.Tv, 12.38.Bx, 13.85.Tp

I. INTRODUCTION

Atmospheric neutrinos and muons are the most important source of background for present and future neutrino telescopes, which are expected to open a new window in astronomy by detecting neutrinos from astrophysical sources.

At energies above 1 TeV, atmospheric lepton fluxes have a prompt component consisting of neutrinos and muons created in semileptonic decays of charmed particles, as opposed to the conventional leptons coming from decays of pions and kaons. Thus a model for charm production and decays in the atmosphere is required.

We base our model on QCD, the theoretically preferred model, to compute the charm production. We use a next-to-leading order (NLO) perturbative QCD (PQCD) calculation of charm production in the atmosphere, followed by a full simulation of particle cascades generated with PYTHIA routines [1].

We have already examined the prompt muon and neutrino fluxes in two previous papers [2,3] [called Gelmini-Gondolo-Varieschi (GGV1) and GGV2 from now on].

In our first paper [2], we found that the NLO PQCD approach produces fluxes in the bulk of older predictions (not based on PQCD) as well as of the recent PQCD semianalytical analysis of Pasquali, Reno and Sarcevic [4]. We also explained the reason of the low fluxes of the Thunman-Ingelman-Gondolo (TIG) model [5], the first to use PQCD in this context, which were due to the chosen extrapolation of the gluon partonic distribution function (PDF) at small momentum fractions x, and we confirmed the overall validity of their pioneering approach to the problem.

In our second paper [3], we analyzed in detail the dependence of the fluxes on the extrapolation of the gluon PDF at small x, which, according to theoretical models, is assumed to be a power law with exponent λ,

$$xg(x) \sim x^{-\lambda}, \tag{1}$$

with λ in the range 0–0.5. Particle physics experiments are yet unable to determine the value of λ at $x < 10^{-5}$. We found that the choice of different values of λ at $x < 10^{-5}$ leads to a wide range of final background fluxes at energies above 10^5 GeV.

Because of this result, in GGV2 we suggested the possibility of measuring λ through the atmospheric leptonic fluxes at energies above 10^5 GeV, not the absolute fluxes, because of their large theoretical error, but rather through their spectral index (i.e. the ''slope''). In particular, we now propose to use the slope of the flux of down-going muons.

We want to stress that we are proposing to use *down-going muons*, at energies $E_\mu \gtrsim 100$ TeV, where prompt muons dominate over conventional ones, and not up-going neutrino-induced muons whose flux is orders of magnitude smaller. While an important contribution to up-going muons is expected from astrophysical neutrinos, there is no background for down-going atmospheric muons.

In this paper we further investigate the possibility of measuring λ, in the more general context of an overall error analysis of our model.

We can identify five potential causes of uncertainty in our final results. The first one is the possible presence of large logarithms of the type $\alpha_s \ln p_T^2$ and $\alpha_s \ln s$ [the latter are the so-called ''$\ln(1/x)$'' terms]. The second is the treatment of the multiplicity in the production of $c\bar{c}$ at high energies.

The third one consists of all the sources of uncertainty hidden in the treatment of particle cascades generated by PYTHIA. The fourth one is the uncertainty in the NLO PQCD charm production model we use. This includes the depen-

*Email address: gelmini@physics.ucla.edu
†Present address: Case Western Reserve University, Cleveland, OH. Email address: gondolo@mppmu.mpg.de
‡Email address: variesch@physics.ucla.edu, gvariesc@lmumail. lmu.edu

dence of the fluxes on the three parameters of the model and the PDF's used. The fifth and final one is the choice of the primary cosmic ray flux, which is the input of our simulation. Of all these potential sources of uncertainty we conclude that only the last two are relevant.

We deal with these five potential sources of error in turn. In Sec. II we address the question of the large logarithms $\alpha_s \ln p_T^2$ and $\alpha_s \ln s$, and in Sec. III we analyze the problem of multiplicity in our charm production mechanism.

In Sec. IV we consider the uncertainties due to the cascade generation by PYTHIA and to our NLO PQCD charm production (the core of our analysis). Here we evaluate the errors due to the parameters of the model, errors that affect the charm production cross section, the final differential and integrated fluxes and their spectral indices. We also determine how the final results (fluxes and their spectral indices) are affected by the choice of different extrapolations of the PDF's at $x<10^{-5}$.

We are finally ready in Sec. V to discuss how λ could be measured. We study the dependence on the different extrapolations of λ at $x<10^{-5}$, we consider the spectral indices and, using the discussion of Sec. IV, we provide an estimate of the errors on these indices and examine the feasibility of an experimental determination of λ at $x<10^{-5}$ with neutrino telescopes.

Finally in Sec. VI we discuss the error in the determination of λ coming from the uncertainties in the elemental composition of the cosmic ray flux.

The determination of λ at small $x<10^{-5}$ is important because in this range saturation, unitarity and shadowing effects should become important. The PDF sets we use have been derived without including saturation effects. Even if this procedure seems to work very well in the DESY ep collider HERA regime (where there might be some indications of saturation already; see e.g. [6]), here we are extrapolating the resulting gluon PDF's at even smaller x values where saturation may become important. With respect to unitarity, using the expression of the Froissart bound on the gluon structure functions given in Eq. 31 of Ref. [7] we see that the extrapolated gluon PDF's we use, with $\lambda = 0.4$–0.5, violate this bound at x values between 0.5×10^{-7} and 1×10^{-7}, for the characteristic momenta $Q^2 \simeq m_c^2 \simeq 3$ GeV^2 we have, which corresponds to leptonic energies of $1-2\times10^6$ GeV. Always using the Froissart bound on the gluon PDF as given in the Eq. 31 of Ref. [7], the gluon PDF's extrapolated with $\lambda \leqslant 0.3$ encounter this bound at $x<10^{-8}$, which corresponds to leptonic energies larger than 10^8 GeV, beyond the energy range relevant in this paper. Shadowing of the gluons in the atmospheric nucleons and nuclei, which we have not included here, could decrease the amplitude of the gluon PDF's by about 10% at $x \simeq 10^{-5}$ and up to as much as 30 to 40% at $x \simeq 10^{-7}$ (see e.g. [8]), which would also change the effective value of λ. There are no shadowing effects in the cosmic ray nucleons and nuclei. Only the dominant x of the gluons in the atmosphere is small in our calculation, while the dominant x of the partons in the cosmic rays is large. Thus shadowing effects do not depend on the unknown composition of cosmic rays, but could only be important for the atmospheric partons. The reason for the different characteristic values of x in the target and projectile partons is the following (for more details see GGV2). Because of the steep decrease with increasing energy of the incoming flux of cosmic rays, only the most energetic charm quarks produced count and those come from the interaction of projectile partons carrying a large fraction of the incoming nucleon momentum. Thus, the characteristic x of the projectile parton, x_1, is large. It is $x_1 \simeq O(10^{-1})$. We can, then, inmediately understand that very small parton momentum fractions are needed in our calculation, because typical partonic center of mass energies $\sqrt{\hat{s}}$ are close to the $c\bar{c}$ threshold, $2m_c \simeq 2$ GeV (since the differential $c\bar{c}$ production cross section decreases with increasing $\hat{s}$), while the total center of mass energy squared is $s=2m_N E$ (with m_N the nucleon mass, $m_N \simeq 1$ GeV). Calling x_2 the momentum fraction of the target parton (in a nucleus of the atmosphere), then, $x_1 x_2 \equiv \hat{s}/s = 4m_c^2/(2m_N E) \simeq \mathrm{GeV}/E$. Thus, $x_2 \simeq O(\mathrm{GeV}/0.1E)$, where E is the energy per nucleon of the incoming cosmic ray in the laboratory frame. The characteristic energy E_c of the charm quark and the dominant leptonic energy E_l in the fluxes are $E_l \simeq E_c \simeq 0.1E$; thus, $x_2 \simeq O(\mathrm{GeV}/E_l)$.

II. IMPORTANCE OF THE $\alpha_s \ln(1/x)$ TERMS

We address here a concern that has been expressed to us several times, about the applicability of perturbative QCD calculations, mostly done for accelerator physics, to the different kinematic domain of cosmic rays.

Contrary to the case in accelerators, we do not have the uncertainty present in the differential cross sections [9] when the transverse momentum p_T is much larger than m_c, uncertainty which is due to the presence of large logarithms of $(p_T^2+m_c^2)/m_c^2$. The reason is that we do not have a forward cut in acceptance, and so the characteristic transverse charm momentum in our simulations is of the order of the charm mass, $p_T \simeq O(m_c)$, and not $p_T \gg O(m_c)$ as in accelerator experiments.

We may, however, depending on the steepness of the gluon structure function λ, have large logarithms of the type $\alpha_s \ln s$, known as ''$\ln(1/x)$'' terms (here $x \simeq \sqrt{4m_c^2/s}$ is the average value of the hadron energy fraction needed to produce the $c\bar{c}$ pair at hadronic center of mass energy squared s). These ''$\ln(1/x)$'' terms arise when the t-channel gluon exchange becomes large, and eventually they have to be resummed. Although techniques exist for resumming these logarithms [10], we have not done it. On the other hand, we have phenomenologically altered the behavior of the parton distribution functions at small x by imposing a power law dependence of the form $xf(x) \sim x^{-\lambda}$. This is analogous to resumming the $\ln(1/x)$ terms in a universal fashion and absorbing them in an improved evolution equation for the gluon density [such as the Balitskiĭ-Fadin-Kuraev-Lipatov (BFKL) evolution equation] [11], a procedure which increases λ. For sufficiently large λ, the large $\ln(1/x)$ terms should not be present.

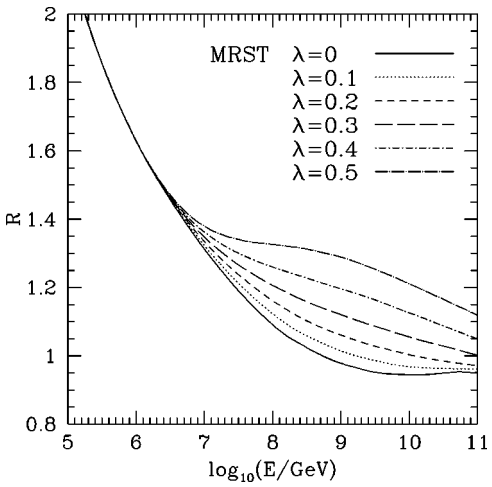

FIG. 1. The ratio $R=(\sigma_{NLO}-\sigma_{LO})/[\sigma_{LO}\alpha_s \ln(s/m_c^2)/\pi]$ is plotted as a function of the beam energy E, for the different values of λ used with the MRST PDF.

To find if our NLO $c\bar{c}$ cross sections are dominated by the $\ln(1/x)$ terms, we have used the following qualitative criterion [12]. We have plotted the ratio

$$R=\frac{\sigma_{NLO}-\sigma_{LO}}{\sigma_{LO}\alpha_s \ln(s/m_c^2)/\pi} \tag{2}$$

as a function of the beam energy E. If the ratio is constant, we are dominated by the $\ln(1/x)$ terms, and if it decreases, we are not. The good behavior is a decreasing R. Figure 1 shows indeed that up to highest energy we consider in this paper, i.e. 10^{11} GeV, R decreases for $\lambda \gtrsim 0.2$, but is roughly constant for smaller λ's. This indicates that we are not dominated by the $\ln(1/x)$ terms provided $\lambda \gtrsim 0.2$.

Clearly, this test involving the R ratio does not say anything about $\ln(1/x)$ higher order corrections. One can only argue that if the $\ln(1/x)$ terms are not dominant at NLO (for R decreasing with energy), the corresponding $[\ln(1/x)]^n$ terms may also be non-dominant in higher order corrections. In any event, the data on charm production that could be inferred at $x<10^{-5}$, from the slope of atmospheric muon fluxes, really give information on the product of the gluon PDF and the parton cross section and a measurement of this product is useful. One can expect that the $\ln(1/x)$ terms at higher order may be better understood by the time the data will come.

III. MULTIPLICITY IN CHARM PRODUCTION

Another concern is the fact that at high energies the charm production cross section we use is sometimes larger than the total pp cross section. At first sight this seems absurd, but we show here that the cross section we use is the inclusive cross section, which contains the charm multiplicity; i.e., it counts the number of $c\bar{c}$ pairs produced, and so can be larger than the total cross section. On the other hand, the contribution of $c\bar{c}$ producing events to the total pp cross section, i.e. the cross section for producing at least one $c\bar{c}$ pair is always smaller than the total pp cross section.

We call σ_{QCD} the perturbative QCD cross section of $c\bar{c}$ pair production in pp collisions,

$$\sigma_{QCD}=\sum_{ij} \sigma_{QCD}(ij\to c\bar{c}), \tag{3}$$

where the sum is over the partons i and j in the colliding nucleons, and

$$\sigma_{QCD}(ij\to c\bar{c})=\int dx_1 dx_2 dQ^2 \frac{d\hat{\sigma}(ij\to c\bar{c})}{dQ^2} \times f_i(x_1,\mu_F^2) f_j(x_2,\mu_F^2). \tag{4}$$

Here $d\hat{\sigma}(ij\to c\bar{c})/dQ^2$ is the $ij\to c\bar{c}$ parton scattering cross section, Q^2 is the four-momentum transfer squared, x_i is the fraction of the momentum of the parent nucleon carried by parton i, and $f_i(x,\mu_F^2)$ is the usual parton distribution function for parton momentum fraction x and factorization scale μ_F.

In the scattering of each pair of partons (one parton from the target and one from the projectile) only one $c\bar{c}$ pair may be produced, but the number of parton pairs interacting in each nucleon-nucleon collision is in general not limited to 1 and it increases with the number of partons $f(x,\mu_F^2)dx$ in each nucleon.

For λ close to 0.5, σ_{QCD} becomes larger than the total pp cross section $\sigma_{pp}\sim 200$ mb at $E_p\sim 10^{10}$ GeV. It is obvious therefore that our results at high energy and large λ are unphysical, unless multiplicity is taken into account. In fact, multiparton interactions should be taken into account already at a smaller cross section of order 10 mb, as determined in studies of double parton scattering [13].

In order to incorporate multiparton scatterings into our analysis, we use an impact-parameter representation for the scattering amplitude and ignore spin-dependent effects (cf. [14]). Assuming the validity of factorization theorems, the mean number of parton-parton interactions $ij\to c\bar{c}$ in the collision of two protons at impact parameter $\vec{b}$ is given by

$$n_{c\bar{c}}(\vec{b})=\sum_{ij} \int d^2b' dx_1 dx_2 dQ^2 \frac{d\hat{\sigma}(ij\to c\bar{c})}{dQ^2} \times f_i(x_1,\mu_F^2,\vec{b}') f_j(x_2,\mu_F^2,\vec{b}+\vec{b}'), \tag{5}$$

where $f_i(x,\mu_F^2,\vec{b})d^2b$ is the number of partons i in the interval $(x,x+dx)$ and in the transverse area element d^2b at a distance $\vec{b}$ from the center of the proton. For simplicity of notation we drop the vector symbol in $\vec{b}$ and write b from now on.

If $n_{c\bar{c}}(b)\ll 1$, $n_{c\bar{c}}(b)$ is the probability of producing a $c\bar{c}$ pair in a pp collision at impact parameter b. If $n_{c\bar{c}}(b)\gtrsim 1$, $n_{c\bar{c}}(b)$ is just the mean value of k, the number of $c\bar{c}$ pairs

produced, at impact parameter b. Let the probability of k scatterings $ij \to c\bar{c}$ in a pp collision at impact parameter b be $P_{kc\bar{c}}(b)$. Then

$$n_{c\bar{c}}(b) = \sum_{k=0}^{\infty} k P_{kc\bar{c}}(b). \tag{6}$$

The k-tuple parton cross section is obtained by integrating the probability of exactly k parton scatterings $P_{kc\bar{c}}(b)$ over the impact parameter b,

$$\sigma_{kc\bar{c}} = \int d^2b P_{kc\bar{c}}(b); \tag{7}$$

the inclusive cross section for charm production is, thus, $\sigma_{c\bar{c}\,\mathrm{incl}} = \Sigma_k k \sigma_{kc\bar{c}}$ and the contribution of charm producing processes to the total cross section is $\sigma_{c\bar{c}} = \Sigma_k \sigma_{kc\bar{c}}$ for $k \neq 0$.

In our evaluation of charm production by cosmic ray interactions in the atmosphere, we must count the number of $c\bar{c}$ pairs produced in the pp collision. So we are precisely interested in the inclusive cross section $\sigma_{c\bar{c}\,\mathrm{incl}}$, which includes the number k of $c\bar{c}$ pairs produced per collision (the multiplicity). We find

$$\sigma_{c\bar{c}\,\mathrm{incl}} = \sum_k k \sigma_{kc\bar{c}} = \int d^2b \sum_k k P_{kc\bar{c}}(b) = \int d^2b\, n_{c\bar{c}}(b). \tag{8}$$

This cross section can be larger than the total pp cross section, because it accounts for multiparton interactions. In particular, using $\sigma_{c\bar{c}}$, the contribution of charm producing processes to the total cross section defined above, the ratio $\sigma_{c\bar{c}\,\mathrm{incl}}/\sigma_{c\bar{c}}$ gives the average charm multiplicity.

Notice that here we consider only independent production of $c\bar{c}$ pairs, so that from each pair of colliding partons it results only one $c\bar{c}$ pair, and we neglect coherent production of multiple $c\bar{c}$ pairs in $2 \to 4$, $2 \to 6$, etc., processes. This will underestimate the charm production cross section.

We assume in the following that the partonic distributions $f_i(x, \mu_F^2, b)$ factorize as

$$f_i(x, \mu_F^2, b) = f_i(x, \mu_F^2) \rho_i(b), \tag{9}$$

where $f_i(x, \mu_F^2)$ is the usual parton distribution function, and $\rho_i(b)$ is the probability density of finding a parton in the area d^2b at impact parameter b. We normalize $\rho_i(b)$ to $\int d^2b\ \rho_i(b) = 1$, to maintain the usual normalization $\int dx\ x f_i(x) = 1$. The factorization in Eq. (9) is consistent with the usual parton picture and with our assumption of no parton-parton correlations.

The mean number of $ij \to c\bar{c}$ scatterings at impact parameter b then becomes

$$n_{c\bar{c}}(b) = \sum_{ij} a_{ij}(b) \sigma_{QCD}(ij \to c\bar{c}), \tag{10}$$

where

$$a_{ij}(b) = \int d^2b' \rho_i(b') \rho_j(b + b') \tag{11}$$

is an overlap integral, and $\sigma_{QCD}(ij \to c\bar{c})$ is the QCD parton-parton cross section for $ij \to c\bar{c}$, as in Eq. (4). From the normalization of $\rho_i(b)$ it follows that $\int d^2b a_{ij}(b) = 1$ for every i, j. Hence from Eqs. (8) and (10) we find

$$\sigma_{c\bar{c}\,\mathrm{incl}} = \sigma_{QCD}, \tag{12}$$

where σ_{QCD}, given in Eq. (3), is the charm production cross section calculated within QCD. This justifies our use of σ_{QCD} as $\sigma_{c\bar{c}\,\mathrm{incl}}$ in the calculation of the atmospheric fluxes.

The way in which we use $\sigma_{c\bar{c}\,\mathrm{incl}}$ in our simulation is as follows. We input only one $c\bar{c}$ pair per pp collision at a given energy E, and multiply the outcome by $\sigma_{c\bar{c}\,\mathrm{incl}}$, which includes the $c\bar{c}$ multiplicity. We make, therefore, the following approximation in the kinematics of the $c\bar{c}$ pairs produced in the same pp interaction. Even if in a real multiparton collision the energy available to the second and other $c\bar{c}$ pairs is smaller than E, we are neglecting this difference. This is a very good approximation because the fraction of center of mass energy that goes into a $c\bar{c}$ pair is of the order of $\sqrt{\hat{s}/s} \sim \sqrt{10\ \mathrm{GeV}/E} \ll 1$ at the high energies we are concerned with.

Although we have explicitly proved Eq. (12) in the absence of parton-parton correlations, the same result can be obtained when correlations are present (see Sec. V of Ref. [15] and references therein). What is proved even in the presence of correlations is that the PQCD single scattering cross section σ_{QCD} is equal to the average number of parton-parton collisions, call it $\langle N \rangle$, multiplied by the contribution of $c\bar{c}$ producing events to the total cross section (the cross section $\sigma_{c\bar{c}}$ defined above), namely $\sigma_{QCD} = \langle N \rangle \sigma_{c\bar{c}}$ (while the inclusive cross section is equal to the average multiplicity of $c\bar{c}$ pairs multiplied by $\sigma_{c\bar{c}}$). Here $\langle N \rangle$ may in general contain contributions from two types of collisions. One type consists of collisions of pairs of partons (consisting of one parton from each interacting nucleon) which interact only once at different points of the transverse plane. Each collision of this type results in our case in one $c\bar{c}$ pair produced. The second type consists of rescatterings in which one parton of one of the nucleons and its interaction products interact with several partons of the other nucleon. In interactions of this type, which are much rarer than the first ones, the number of $c\bar{c}$ pairs produced not necessarily coincides with the number of collisions. If rescatterings can be neglected, then $\langle N \rangle$ is the average number of $c\bar{c}$ pairs produced and σ_{QCD} is the inclusive $c\bar{c}$ production cross section as stated in Eq. (12). Otherwise small rescattering corrections, to our knowledge not yet calculated [16], are necessary (rescatterings would also modify the energy spectrum of the particles produced).

IV. UNCERTAINTIES DUE TO CASCADE SIMULATION, PARAMETERS OF CHARM PRODUCTION MODEL AND CHOICE OF PDF'S

In our first paper (GGV1) we considered the uncertainties related to the cascade generation in PYTHIA. There we tried different modes of cascade generation, different options allowed by PYTHIA in the various stages of parton showering, hadronization, interactions and decays, etc., without noticing substantial changes in the final results (differing at most by 10%). These uncertainties are however very difficult to quantify, due to the nature of the PYTHIA routines. Since these uncertainties are small, we neglect them in this analysis and continue to use PYTHIA with the options described in GGV1 as our main choice for the simulation: ''single'' mode with showering, ''independent'' fragmentation, interactions and semileptonic decays according to TIG.

In our ''single'' mode we enter only one c quark in the particle list of PYTHIA, and we multiply the result by a factor of 2 to account for the initial $\bar{c}$ quark. PYTHIA performs the showering, standard independent fragmentation, and follows all the interactions and decays using default parameters and options. In GGV1 we have argued that this ''single'' approach is equivalent to what we called the ''double'' mode, in which both $c\bar{c}$ partons are placed in the initial event list, in the first step of a standard cascade evolution. The ''single'' option is chosen thus because it reduces considerably the computing time.

Important sources of uncertainty are contained in our charm production model, which is NLO PQCD as implemented in the Mangano-Nason Ridolfi (MNR) program [9], calibrated at low energies.

The calibration procedure consisted of the following:

(i) Choosing a PDF set from those available and fixing the related value of Λ_{QCD}.[1]

(ii) Choosing m_c, μ_F and μ_R, which are the charm mass, the factorization scale and the renormalization scale respectively, so as to fit simultaneously both the total and differential cross sections from existing fixed target charm production experiments [17,18] at the energy of 250 GeV, without additional normalization factors.

(iii) Checking that the total cross section generated after the previous choices fits reasonably well the other existing experimental points for fixed target charm production experiments [19].

Besides the choice of the PDF set, our procedure has the freedom to choose reasonable values of the three parameters m_c, μ_F, and μ_R so as to fit the experimental data. In GGV1 and GGV2 we made the standard choice [9,19] of

$$\mu_F = 2m_T, \quad \mu_R = m_T, \tag{13}$$

where $m_T = \sqrt{p_T^2 + m_c^2}$ is the transverse mass. The values of the charm mass are taken slightly different for each PDF set, namely,

$$m_c = 1.185 \text{ GeV} \quad \text{for Martin-Roberts-Stirling set R1 (MRS R1)}, \tag{14}$$

$$m_c = 1.310 \text{ GeV} \quad \text{for MRS R2}, \tag{15}$$

$$m_c = 1.270 \text{ GeV} \quad \text{for CTEQ 4M}, \tag{16}$$

$$m_c = 1.250 \text{ GeV} \quad \text{for MRS-Thorne (MRST)}. \tag{17}$$

Here we explore the changes induced in cross sections and fluxes at high energies by different choices of m_c, μ_F, and μ_R which satisfy our calibration requirements.

We have performed this analysis with the most recent PDF set: the MRST [20] (other PDF's give similar results). At first we fix $\lambda = 0$ and then we examine other values of λ. We note that the calibration procedure described above is independent of λ because it involves only relatively low energies, where the low x extrapolation is not an issue.

A. MRST $\lambda = 0$: Fluxes

We considered the $\lambda = 0$ case because it is the most significant for the evaluation of the uncertainties in the spectral indices, as will be clear in the next subsection. We have considered the following reasonable ranges of the parameters:

$$1.1 \text{ GeV} \leqslant m_c \leqslant 1.4 \text{ GeV}, \tag{18}$$

$$0.5m_T \leqslant \mu_F \leqslant 2m_T, \tag{19}$$

$$0.5m_T \leqslant \mu_R \leqslant 2m_T, \tag{20}$$

where the bounds on m_c come from the 1998 Particle Data Group [21], while those for μ_F and μ_R are those used in the existing literature [9,19].

Within these ranges we have looked for values of the three parameters capable of reproducing the experimental data in our calibration procedure described before. Table I summarizes the different sets of parameters: we have varied the charm mass through the values $m_c = 1.1$, 1.2, 1.25, 1.3, 1.4 GeV [$m_c = 1.25$ GeV was our previous optimal choice for MRST in Eq. (17)] and then, for each value of m_c, we have found values of the factorization and renormalization scales that reproduce the experimental total cross section $\sigma_{c\bar{c}} = 13.5 \pm 2.2 \mu$b at 250 GeV [17]. In particular, for each value of m_c, we took $\mu_F = m_T/2$, m_T, $2m_T$ and then, for each m_c, μ_F pair, found the value of μ_R which best fits the data (see Table I).

We have also checked that these choices give good fits to the differential, besides the total, cross sections at 250 GeV [18], without additional normalization factors, as done for the original choice of parameters in GGV1. For $m_c = 1.1$ GeV we had to choose values of μ_R slightly outside the range in Eq. (20) (but we have kept these values in our analysis anyway).

[1] We note that Λ_{QCD} can be chosen in the MNR program independently of the PDF and therefore can constitute an additional independent parameter of our model. We have opted however to choose the value of Λ_{QCD} assumed in the PDF set being used, for consistency.

TABLE I. Choice of parameters m_c, μ_F and μ_R that can reproduce the experimental total cross section $\sigma_{c\bar{c}}^{expt}$ for charm production in pN collisions at 250 GeV from the E769 experiment. For each set of parameters, $\sigma_{c\bar{c}}^{MNR}$ is the cross section calculated with the MNR program using MRST PDF.

m_c(GeV)	μ_F (m_T)	μ_R (m_T)	$\sigma_{c\bar{c}}^{MNR}$ (μb)	$\sigma_{c\bar{c}}^{expt}$ (μb)
1.1	0.5	2.53	13.48	13.5±2.2
	1.0	2.40	13.48	''
	2.0	2.10	13.42	''
1.2	0.5	1.46	13.57	13.5±2.2
	1.0	1.40	13.54	''
	2.0	1.23	13.51	''
1.25	0.5	1.18	13.57	13.5±2.2
	1.0	1.13	13.54	''
	2.0	1.00	13.58	''
1.3	0.5	0.96	13.55	13.5±2.2
	1.0	0.92	13.50	''
	2.0	0.83	13.53	''
1.4	0.5	0.68	13.51	13.5±2.2
	1.0	0.66	13.51	''
	2.0	0.61	13.52	''

For all the sets of parameters in Table I we have run our full simulations for the MRST, $\lambda=0$ case and the results are described in Figs. 2–4.

In Figs. 2a and 2b we show the resulting total charm production cross section $\sigma_{c\bar{c}}$ for all 15 sets of parameters in Table I, together with recent experimental data (from Table I of Ref. [19], where all the data for pp or pN collisions have been transformed into a $\sigma_{c\bar{c}}$ cross section following the procedure described in GGV1). Figure 2b is an enlargement of the region of Fig. 2a containing the experimental data.

In Fig. 2a we see the spread of the cross sections, which is more than one order of magnitude at 10^{11} GeV. Above 250 GeV, one can clearly distinguish three ''bands'' of increasing cross sections for $\mu_F=m_T/2$, m_T and $2m_T$. Within each ''band'' the cross sections increase with increasing values of m_c (and correspondingly smaller values of μ_R), in Table I. Our standard choice ($m_c=1.25$ GeV, $\mu_F=2m_T$, $\mu_R=m_T$) proves to be one of the highest cross sections we obtain.

In Fig. 2b we see better how all of these cross sections verify our calibration procedure. They pass through the point at 250 GeV [17], agree with the point at 400 GeV [22] and disagree with the very low experimental point at 200 GeV [23]. The lower values of $\mu_F=m_T/2$ and m_T fit better the lowest experimental point at 800 GeV [24], while the higher value of $\mu_F=2m_T$ fits better the upper point at 800 GeV [25].

We believe that the spread of the total cross sections shown in Fig. 2a provides a reasonable estimate of the uncertainty of our charm production model at fixed λ. Since our standard choice of parameters ($m_c=1.25$ GeV, $\mu_F=2m_T$, $\mu_R=m_T$) gives one of the highest cross sections (in better agreement with the more recent value of the cross section at 800 GeV [25]), the uncertainty band should be added under each of the cross section curves calculated with our standard choice of parameters (like the curves shown in Fig. 1 of GGV2).

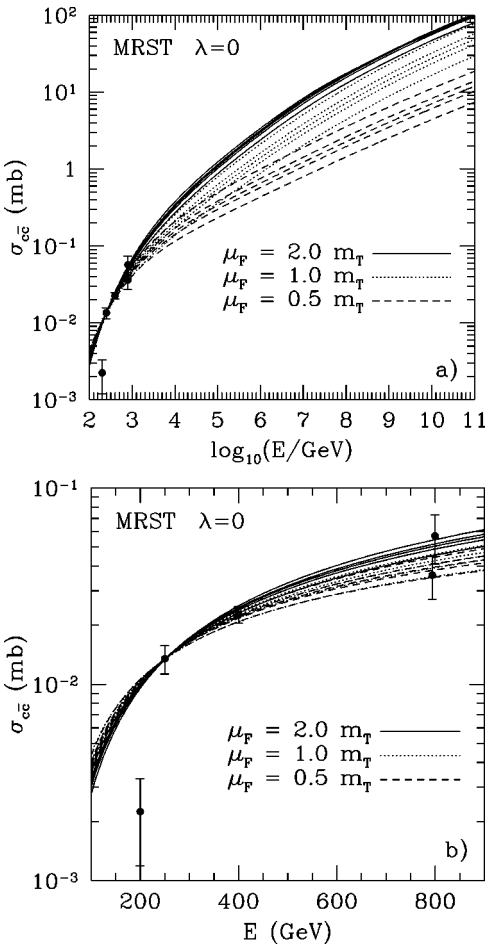

FIG. 2. Total cross sections for charm production $\sigma_{c\bar{c}}$, up to NLO, calculated with MRST ($\lambda=0$) and the values of m_c, μ_F, μ_R of Table I, are compared with recent experimental values [17,19,22–25]. For each ''band'' in the figures (i.e. for $\mu_F=m_T/2$, m_T and $2m_T$) the cross sections increase with increasing m_c (and correspondingly smaller values of μ_R) in Table I [(b) is an enlargement of (a)].

Figure 3 illustrates the corresponding spread of the final prompt fluxes. Although our results are for the MRST PDF's extrapolated with $\lambda=0$ (the value of λ which gives the lowest fluxes) similar spreads result from other PDF's and λ's. We show the flux of muons; the fluxes of muon-neutrinos and electron-neutrinos are essentially the same.

Similarly to what happens with cross sections in Fig. 2, the fluxes in Fig. 3 increase with $\mu_F=m_T/2$, m_T and $2m_T$ and, within each band, they increase with increasing m_c (and correspondingly smaller values of μ_R), in Table I. At energies around 10^6 GeV the total uncertainty is almost one order of magnitude and decreases slightly for higher energies. If we would decide to work only with $\mu_F=2m_T$ (which fits the experimental measurement at 800 GeV with the highest cross section), the uncertainty would be greatly reduced: the fluxes in this rather narrow band differ by less than 40%. We

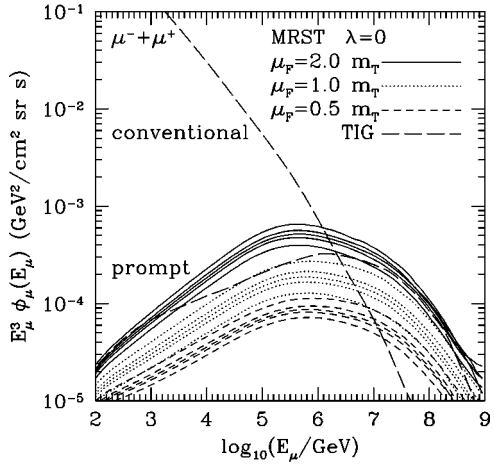

FIG. 3. Results for MRST $\lambda=0$. The E_μ^3-weighted vertical prompt fluxes, at NLO, are calculated using the values of m_c, μ_F, μ_R of Table I and compared to the TIG [5] conventional and prompt fluxes. For each ''band'' in the figure (i.e. for $\mu_F=m_T/2$, m_T and $2m_T$) the fluxes increase with increasing m_c (and correspondingly smaller values of μ_R) in Table I.

observe that the flux calculated with our standard choice of parameters ($m_c=1.25$ GeV, $\mu_F=2m_T$, $\mu_R=m_T$) is almost the highest, as was the case for the corresponding cross section in Fig. 2.

In Fig. 3 we also indicate the conventional and prompt fluxes from TIG; we notice that the TIG prompt flux is within our band of uncertainty, which is reasonable since TIG used a low $\lambda=0.08$ value for their predictions (see the discussions in GGV1 and GGV2).

B. MRST $\lambda=0$: Spectral index

In our previous paper GGV2, we pointed out that an experimental measurement of the slope of the atmospheric lepton fluxes at energies where the prompt component dominates over the conventional one might give information on

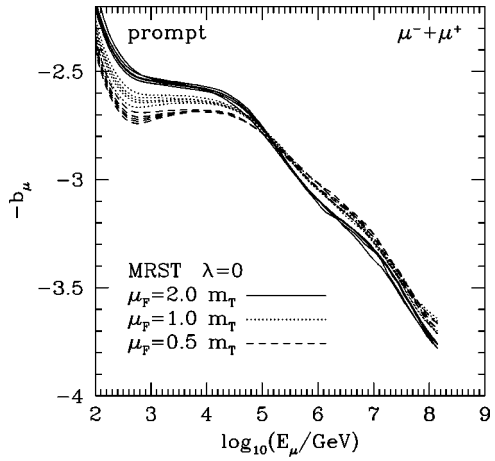

FIG. 4. Spectral indices $-b_\mu$ of the fluxes plotted in Fig. 3, for the MRST $\lambda=0$ case. For each ''band'' in the figure (i.e. for $\mu_F=m_T/2$, m_T and $2m_T$) the spectral indices decrease with increasing m_c (and correspondingly smaller values of μ_R) in Table I.

the value of λ, the slope of the gluon PDF at small x. The best flux for this measurement is that of down-going muons, because the prompt neutrinos have first to convert into muons or electrons through a charged current interaction in order to be detectable in a neutrino telescope.

In this section and in the following two we consider the uncertainties in our method to determine λ. In this section we examine those coming from the charm production model, in Sec. V those related to the non-linearity of our model, and in Sec. VI those coming from the unknown composition of the cosmic rays at high energies.

The slope of the fluxes or spectral index is $\alpha_l(E_l)=-\partial\ln\phi_l(E_l)/\partial\ln E_l$, with $l=\mu^\pm,\nu_\mu+\overline{\nu_\mu}$ or $\nu_e+\overline{\nu_e}$. In other words, the final lepton fluxes are

$$\phi_l(E_l)\propto E_l^{-\alpha_l(E_l)}. \tag{21}$$

In GGV2 we found a simple linear dependence of α_l on λ, namely

$$\alpha_l(E_l)=b_l(E_l,\gamma,\lambda)-\lambda\simeq b_l(E_l)-\lambda, \tag{22}$$

where $b_l(E_l)$ is an energy dependent coefficient evaluated using our simulation with $\lambda=0$ and fixed γ. As argued in GGV2 [cf. Eqs. (35) and (36) therein], the coefficient $b_l(E_l,\gamma,\lambda)$ depends mildly on λ and can be well approximated by its value for $\lambda=0$ (see Sec. V). The coefficient $b_l(E_l,\gamma,\lambda)$ depends almost linearly on γ, the spectral index of the primary cosmic rays. We recall that the equivalent nucleon flux for primary cosmic rays is expressed as

$$\phi_N(E)\propto E^{-\gamma-1}. \tag{23}$$

The linear dependence of $b_l(E_l,\gamma,\lambda)$ on γ can be written as

$$b_l(E_l,\gamma,\lambda)=\overline{b_l}(E_l,\gamma,\lambda)+\gamma, \tag{24}$$

where $\overline{b_l}(E_l,\gamma,\lambda)$ depends mildly on λ and γ,[2] as we will prove in Secs. V and VI, respectively.

Given $b_l(E_l)$ from our model, an experimental measurement of α_l at energy E_l would immediately give λ corresponding to a value of $x\simeq \mathrm{GeV}/E_l$, as we discussed in GGV2. A measurement at $E_l\simeq 10^6$ GeV$=1$ PeV would give λ at $x\simeq 10^{-6}$, a value of x unattainable by present experiments.

For the time being we keep fixed the value of γ ($\gamma=1.7$ below the knee and $\gamma=2.0$ above the knee, as in GGV1 and GGV2); only in Sec. VI will we consider changes in the value of γ.

The feasibility of a measurement of λ depends, therefore, on the uncertainties in $b_l(E_l)$. Here we discuss those coming from the charm production model.

Figure 4 shows the $-b_\mu$ corresponding to the fluxes of Fig. 3 as functions of E_μ. In the region of interest, E_μ

[2]We have included in $\overline{b_l}$ the $+1$ term coming from the -1 in the exponent of Eq. (23).

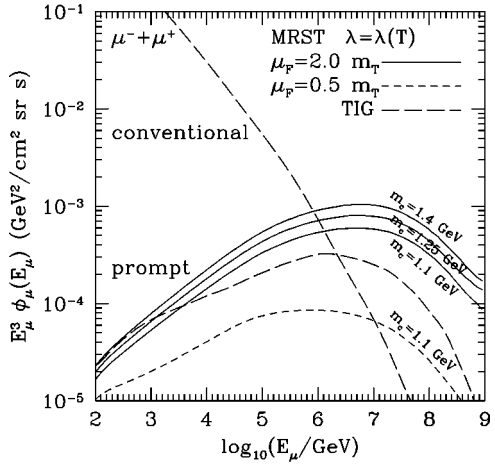

FIG. 5. Results for MRST $\lambda=\lambda(T)$. The E_μ^3-weighted vertical prompt fluxes, at NLO, are calculated using selected values of m_c, μ_F, μ_R from Table I and compared to the TIG [5] conventional and prompt fluxes.

$\gtrsim 10^5$–10^6 GeV, the values of $-b_\mu$ within each ''band'' decrease with increasing m_c (and correspondingly smaller values of μ_R), in Table I.

The spread of b_μ due to the choice of μ_F, μ_R and m_c is $\Delta b_\mu \simeq 0.1$, or $\Delta b_\mu / b_\mu \simeq 0.03$, much smaller than the uncertainty $\Delta\phi_\mu/\phi_\mu \simeq 10$ of the absolute flux in Fig. 3. If we would for some reason restrict ourselves to the $\mu_F = 2\ m_T$ band, the uncertainty on b_μ would become even smaller, $\Delta b_\mu \simeq 0.03$. We will refer to this error as Δb_{par} in the following, as it is related to the choice of parameters in the charm production model, and consider half of the spread in Fig. 4 to evaluate it. Therefore

$$\Delta b_{par} \simeq 0.05\ \ (0.015), \tag{25}$$

where the value in parenthesis corresponds to the $\mu_F = 2m_T$ band.

C. MRST $\lambda=\lambda(T)$

So far we used $\lambda=0$ only. This case determines the uncertainty of the $b_l(E_l)$ function which enters in the determination of λ through the atmospheric muon fluxes.

Here we study an ''intermediate'' value of λ. We continue to use the MRST PDF, but with the value of $\lambda=\lambda(T)$ given by the slope of the lowest tabulated value of x (see GGV2 for more explanations). This value depends on Q^2 and is about 0.2–0.3.

We repeat the same analysis of Sec. IV A. However, for simplicity, we report the results for four selected sets of values for the parameters in Table I. The first set ($m_c=1.1$ GeV, $\mu_F=0.5\ m_T$, $\mu_R=2.53\ m_T$) gives a lower bound for the fluxes. The second set ($m_c=1.4$ GeV, $\mu_F=2m_T$, $\mu_R=0.61\ m_T$) gives an upper bound for the fluxes. The remaining two sets are cases in the $\mu_F=2m_T$ ''band.''

The results are plotted in Fig. 5. The general features of Fig. 5 coincide with those of Fig. 3, except for an overall increase in all the fluxes due to the larger value of λ. The total spread of the fluxes given by the two limiting cases and the spread within the narrower $\mu_F=2m_T$ band are comparable to those found for $\lambda=0$. As in Fig. 3, our standard choice of parameters ($m_c=1.25$ GeV, $\mu_F=2m_T$, $\mu_R=1.0m_T$) yields almost the highest flux.

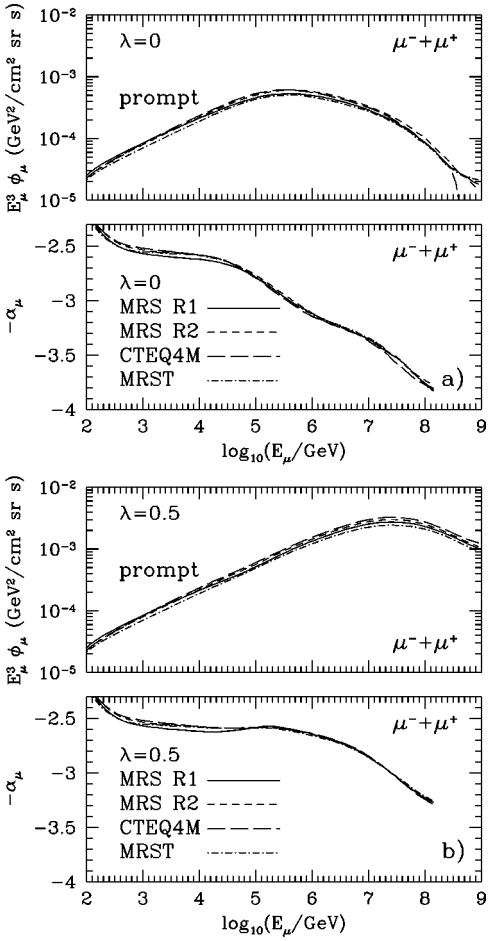

FIG. 6. Results for MRS R1-R2, CTEQ 4M, MRST, for $\lambda=0$ (a) and $\lambda=0.5$ (b), with standard choice of parameters m_c, μ_F, μ_R. Top part: E_μ^3-weighted vertical prompt fluxes, at NLO. Bottom part: related spectral indices $-\alpha_\mu$ (for the $\lambda=0$ case, $-\alpha_\mu=-b_\mu$).

We conclude that similar features would be obtained for other values of λ: our ''standard choice'' flux would be almost the highest in a band of uncertainty whose width is similar for all values of λ. The fluxes in the uncertainty band of Fig. 5 are consistent with older predictions (see GGV1 and references therein) and with the prediction by Pasquali *et al.* [4].

D. Other PDF's

Another source of uncertainty for the final fluxes and spectral indices is the choice of the PDF set. As in GGV2, we consider here four recent sets of PDF's: MRS R1-R2 [26], CTEQ 4M [27] and MRST [20], with the standard choice of parameters of Eqs. (13), (14), (15), (16), (17).

Figures 6a and 6b show the muon fluxes (top panels) and spectral indices (bottom panels) for the two limiting cases of $\lambda=0$ (Fig. 6a) and $\lambda=0.5$ (Fig. 6b). In both cases the μ

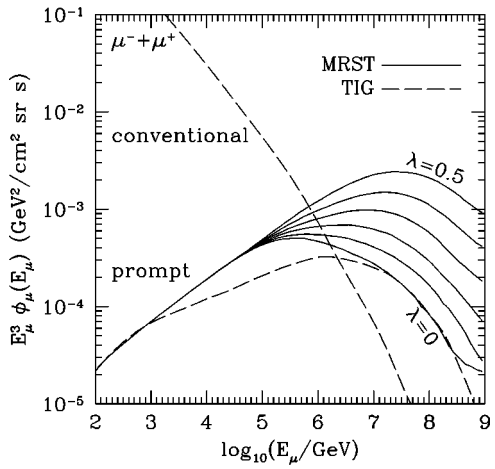

FIG. 7. Results for MRST $\lambda=0-0.5$ (solid lines). The E_μ^3-weighted vertical prompt fluxes, at NLO, are compared to the TIG [5] conventional and prompt fluxes (dashed lines).

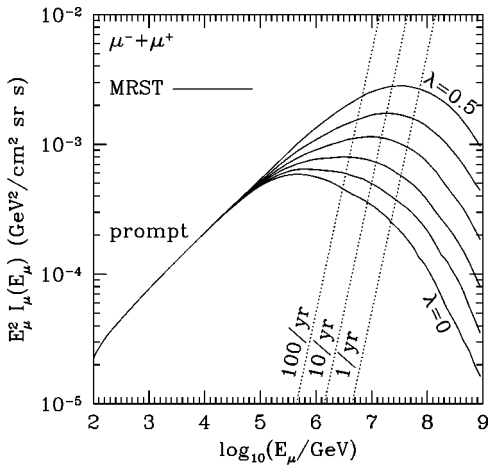

FIG. 8. Results for MRST $\lambda=0-0.5$ (solid lines). The E_μ^2-weighted integrated vertical prompt fluxes, at NLO, are compared to the number of particles traversing a km^3 2π sr detector per year (dotted lines).

fluxes show at most a 30%–50% variation depending on the PDF used. The uncertainty in the spectral indices for $E_\mu \gtrsim 10^5$–10^6 GeV is $\Delta b_\mu \lesssim 0.02$, or $\Delta b_\mu / b_\mu \lesssim 0.01$. This error will be denoted as Δb_{PDF} in the following, namely (again dividing the spread by 2)

$$\Delta b_{PDF} \simeq 0.01. \tag{26}$$

These uncertainties, related to the PDF's, are smaller that those due to the choices of mass scales (see Figs. 3 and 4). We conclude that, provided different PDF's are calibrated in a similar way (i.e. same values of μ_F, μ_R and m_c, chosen to fit the experimental data of our calibration), the final fluxes and spectral indices are very similar. The main source of uncertainty resides therefore in the choice of the mass parameters, rather than the adoption of a certain PDF set.

V. DETERMINATION OF λ WITH NEUTRINO TELESCOPES

In GGV2 we have given a detailed analysis of the dependence of the final fluxes and spectral indices on λ for different PDF's. In this section we show that the spread in our results due to λ is larger than the one due to the choice of μ_F, μ_R, m_c and of the PDF set, analyzed in the previous section. This is good news for the possibility of measuring λ, since the spread in α_μ, due to different λ's, is the signal we want to detect, while the spread due to other factors constitutes the theoretical error of this measurement.

Figures 7–10 show how the μ flux and its spectral index depend on λ. We used MRST with variable $\lambda = 0,0.1,0.2,0.3,0.4,0.5$ and our standard choice of parameters ($m_c = 1.25$ GeV, $\mu_F = 2m_T$, $\mu_R = 1.0\ m_T$).

Figure 7 contains the differential muon fluxes. At the highest energies the μ fluxes are spread over almost two orders of magnitude. To each of the curves in this plot we need to assign a band of uncertainty of about one order of magnitude coming from the choice of the PDF and of the parameters m_c, μ_F, and μ_R (see Fig. 3). Thus the curves become entirely superposed with each other. This makes it impossible to derive the value of λ from an experimental measurement of the absolute level of the fluxes. However, the uncertainties in the spectral index of these prompt muons are much smaller and a determination of λ becomes possible using the slope of the muon fluxes instead of their absolute level.

Figure 8 shows the E^2-weighted integrated fluxes as functions of the muon energy. The slant lines indicate the number of particles traversing a km^3 detector over a 2π sr solid angle. Even for the highest predicted fluxes, less than 1 particle per year will traverse the km^3 detector for energies above 10^8 GeV. Moreover, while prompt muons can be detected directly, prompt neutrinos have first to convert into charged leptons before being detected. The smallness of the charged current interaction effecting the conversion considerably lowers the detection rate of neutrinos. Therefore, the slope of the charm component of the atmospheric leptons can be studied in neutrino telescopes only using atmospheric

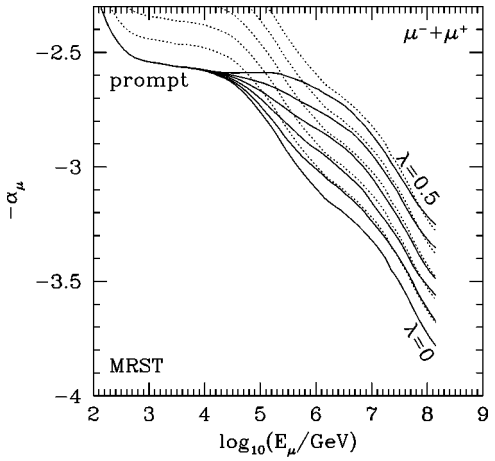

FIG. 9. Results for MRST $\lambda=0-0.5$. The spectral indices $-\alpha_l(E_l)$ for the different values of λ, calculated directly by our simulation (solid lines) are compared to the corresponding terms $-b_l(E_l)+\lambda$ (dotted lines).

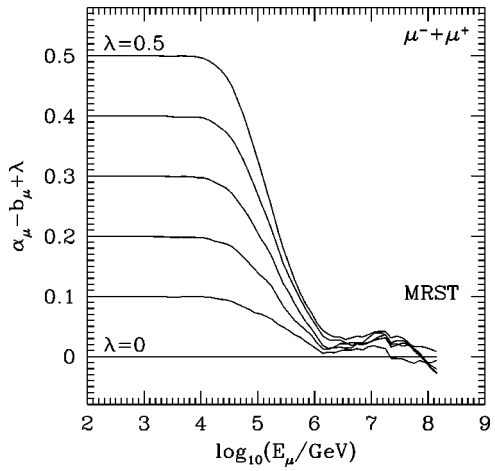

FIG. 10. Results for MRST $\lambda=0-0.5$ (solid lines). The error of Eq. (22) is evaluated in terms of the difference $\alpha_l(E_l)-b_l(E_l)+\lambda$.

muons coming from above the horizon, and only in a narrow range of energies, between a lower limit of $E_\mu \simeq 10^5$–10^6 GeV, above which the prompt component dominates over the conventional one, and an upper limit of $E_\mu \simeq 10^7$–10^8 GeV, above which the detection rates become negligible.

In practice, the spectral index of the prompt muon flux may be estimated by the difference of two integrated muon fluxes above two different energies, e.g. 10^6 and 10^7 GeV.

Figures 9 and 10 prove the validity in our model of Eq. (22), which is $\alpha_l(E_l)=b_l(E_l)-\lambda$. In Fig. 9 we plot the spectral indices $-\alpha_l(E_l)$ for the different values of λ, both as directly calculated with our simulation (solid lines) and as $-b_l(E_l)+\lambda$ (dotted lines), where $b_l(E_l)$ is α_l with $\lambda=0$. The two almost coincide, in the interval of interest, $E_l \gtrsim 10^6$ GeV. Their difference, $\alpha_l(E_l)-b_l(E_l)+\lambda$, given in Fig. 10, is small, about $\simeq 0.03$ at $E \gtrsim 10^6$ GeV. This difference stems from the mild dependence of $b_l(E_l)$ on λ and needs to be added to the the other uncertainties evaluated in Sec. IV. We will refer to this error, due to the non-linearity in λ of Eq. (22), as

$$\Delta b_{non\text{-}lin} \simeq 0.015, \tag{27}$$

which again is evaluated dividing by 2 the spread in Fig. 10.

We see in Fig. 9 that $\Delta\lambda \sim \Delta\alpha$; therefore, we would need an uncertainty in the spectral index of order 0.1 to determine λ with the same accuracy. We will show now that this is roughly the uncertainty related to our theoretical model.

In fact, we can finally estimate the total uncertainty in the determination of λ coming from our theoretical model (that is, excluding the uncertainty due to the unknown composition of cosmic rays). We sum together the three spreads of $b_l(E_l)$ previously calculated in Eqs. (25), (26) and (27), to obtain the final uncertainty,[3] from the charm production model,

$$(\Delta\lambda)_{charm} \simeq (\Delta b_\mu)_{charm} \simeq 0.075 \ \ (0.04), \tag{28}$$

where the number in parentheses corresponds to fixing $\mu_F = 2m_T$ in the charm model.

If the theoretical uncertainties so far presented would be the only ones affecting the determination of λ through a measurement of the slope of the down-going muon flux, we could expect to get to know λ with an uncertainty of about $\Delta\lambda \sim 0.1$. However, even excluding experimental uncertainties in the neutrino telescopes themselves, the uncertainty increases when our ignorance of the composition of the cosmic rays at high energy is taken into account, as we show in the following section.

VI. UNCERTAINTY FROM COSMIC RAY COMPOSITION

The final uncertainty we consider in the determination of λ comes from the poorly known elemental composition of the high energy cosmic rays.

The spectral index of the cosmic rays γ enters almost linearly in the slope of the atmospheric leptons. From Eqs. (22) and (24) we have

$$\alpha_l(E_l) = \overline{b_l}(E_l, \gamma, \lambda) + \gamma - \lambda. \tag{29}$$

So far we have kept γ fixed; thus, the uncertainty Δb_μ calculated in Eq. (28) is actually an uncertainty in $\overline{b_\mu}$. We are going now to evaluate the uncertainty due to γ.

The non-linearity of Eq. (29) with respect to γ is mild, as we have argued analytically in Sec. V of GGV2 and we show here using our numerical simulation. We have conducted a few trial runs of our simulation simply changing the values of γ used for the primary flux. We recall from Sec. IV B that in our model we used $\gamma=1.7,2.0$, respectively below and above the knee at $E=5\times10^6$ GeV. We have run our simulation changing these values of γ by $\pm0.1, \pm0.2$,[4] both above and below the knee, to see the error produced when taking $\overline{b_l}$ computed at fixed γ (our usual values) in Eq. (29) and thus leaving a pure linear dependence on γ. We used the MRST PDF, with $\lambda=0$, but similar results are obtained with other PDF's and λ's.

In Fig. 11a we plot the spectral index $-\alpha_l(E_l)$ for the different values of γ, both as directly calculated with our simulation (solid lines) and as $-\overline{b_l}(E_l;\gamma=1.7,2.0;\lambda=0) - \gamma$ (dotted lines), i.e. using our standard values for γ of the primary flux and adding an increment in γ equal to ±0.1, ±0.2. In this way the ''central value'' of these spectral indices corresponds to the $\lambda=0$ case of Fig. 9. We can see that the dotted and the solid lines almost coincide, especially in the interval of interest for $E_l \gtrsim 10^5$–10^6 GeV, proving the validity of Eq. (29). The uncertainty in $\overline{b_l}$ due to this non-linearity, which we call $\Delta\gamma_{non\text{-}lin}$, evaluated in terms of the difference $\alpha_l - \overline{b_l} - \gamma$, is plotted in Fig. 11b and, in the energy range of interest, is

[3]We summed the errors linearly. Summing in quadrature would give $(\Delta\lambda)_{charm} \simeq (\Delta b_\mu)_{charm} \simeq 0.053$ (0.023).

[4]Notice that these values of γ are some of the most probable values (see Fig. 13).

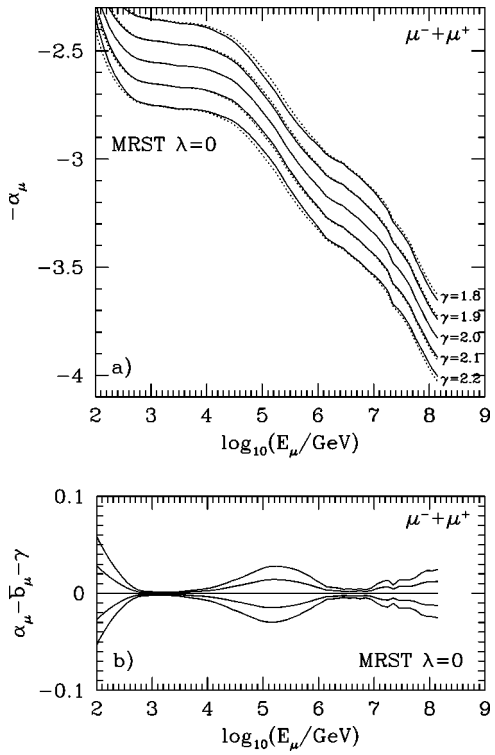

FIG. 11. Results for MRST $\lambda=0$ for different values of γ. (a) The spectral indices $-\alpha_l(E_l)$ for the different values of γ, calculated directly by our simulation (solid lines), are compared to the corresponding terms $-\overline{b_l}(E_l;\gamma=1.7,2.0;\lambda=0)-\gamma$, with increments in γ equal to ± 0.1, ± 0.2 (dotted lines). The curves are labeled by the related value of γ above the knee ($\gamma=2.0$ is our ''standard value''). (b) Uncertainty due to the non-linearity of Eq. (29), as the difference $\alpha_l-\overline{b_l}-\gamma$.

$$\Delta\gamma_{non\text{-}lin}\simeq 0.02. \tag{30}$$

We will now consider the error due to the poorly known elemental composition of the high energy cosmic rays. Concerning charm production, the relevant cosmic ray flux to be considered is the equivalent flux of nucleons impinging on the atmosphere. For a given cosmic ray flux, the equivalent flux of nucleons $\phi_{eq}(E_N)$ depends in general on the composition of the cosmic rays. Nuclei with atomic number A and energy E_A, coming with a flux $\phi_A(E_A)$, contribute an amount $A\phi_A(AE_N)$ to the equivalent flux of nucleons at energy $E_N=E_A/A$. So, in total,

$$\phi_{eq}(E_N)=\sum_A A\phi_A(AE_N). \tag{31}$$

The uncertainties in the equivalent nucleon flux arise from the poorly known composition of cosmic rays in the energy range above the so-called knee, $E_A\sim 10^6$ GeV.

The actual γ that enters into our proposed determination of λ is the spectral index of the equivalent nucleon flux γ_{eq}, the equivalent cosmic ray spectral index for short. The equivalent nucleon flux is written as $\phi_{eq}\propto E_N^{-\gamma_{eq}-1}$, so that the spectral index γ_{eq} is given by

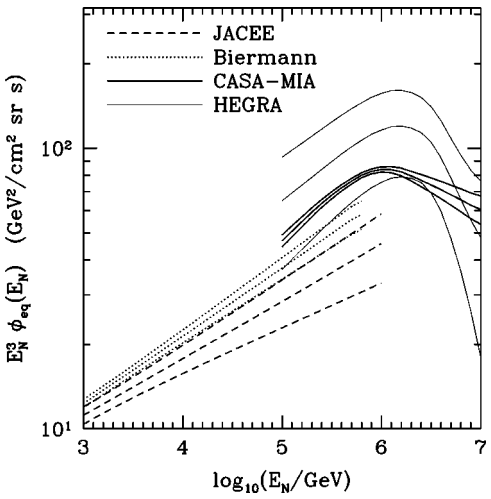

FIG. 12. The E_N^3-weighted equivalent nucleon flux $\phi_{eq}(E_N)$ is shown for different primary cosmic ray experiments [28–31]. For each of these we plot the central value and the related error band.

$$\gamma_{eq}+1=-\frac{E_N}{\phi_{eq}}\frac{\partial\phi_{eq}}{\partial E_N}=\frac{1}{\phi_{eq}}\sum_A A\phi_A(\gamma_A+1), \tag{32}$$

where γ_A is the spectral index of the component of atomic number A, i.e. $\phi_A(E_A)=k_A E_A^{-\gamma_A-1}$.

We have calculated ϕ_{eq} and γ_{eq} using the experimental data of JACEE [28], CASA-MIA [29], HEGRA [30], and the data collected by Wiebel-Sooth *et al.*, in Table I of Ref. [31], each with their respective compositions. Figures 12 and 13 show the ϕ_{eq} and the γ_{eq} so obtained. Only the data of CASA-MIA [29] and HEGRA [30] reach energies $E_N\lesssim 10^8$ GeV, so we have not extended our analysis beyond 10^8 GeV.

We have calculated the error band associated to γ_{eq} in two different ways, because of the different parametrization

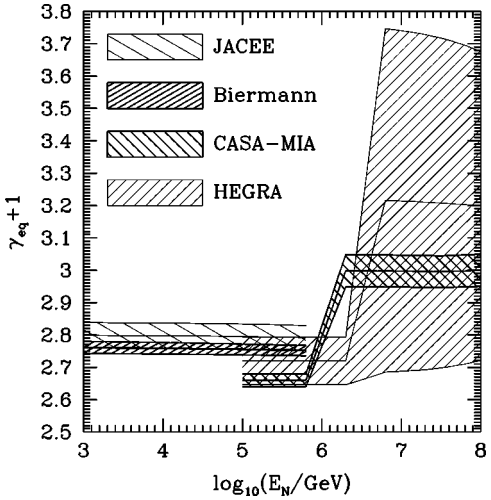

FIG. 13. The spectral index, $\gamma_{eq}+1$, for the equivalent nucleon fluxes of Fig. 12, is shown for different primary cosmic ray experiments [28–31]. For each of these we plot the central value and the related error band.

of the composition used in Refs. [28] to [31]. References [28,31] give separate power law fits to the spectrum of each cosmic ray component,

$$\phi_A(E_A) = k_A E_A^{-\gamma_A - 1}, \tag{33}$$

where the parameters k_A and γ_A have errors Δk_A and $\Delta\gamma_A$. Standard propagation of errors gives, in this case,

$$\Delta\phi_{eq} = \left\{ \sum_A A^2 \phi_A^2 \left[\left(\frac{\Delta k_A}{k_A} \right)^2 + [\ln(AE_N)\Delta\gamma_A]^2 \right] \right\}^{1/2} \tag{34}$$

and

$$\Delta\gamma_{eq} = \left\{ \sum_A \frac{A^2\phi_A^2}{\phi_{eq}^2} \left[(\gamma_A - \gamma_{eq})^2 \left(\frac{\Delta k_A}{k_A} \right)^2 + [1 - (\gamma_A - \gamma_{eq})\ln(AE_N)]^2 (\Delta\gamma_A)^2 \right] \right\}^{1/2}, \tag{35}$$

where ϕ_A is evaluated at $E_A = AE_N$.

References [29,30] give a power law fit to the total particle flux

$$\phi(E_A) = kE_A^{-\gamma - 1} \tag{36}$$

and a composition ratio $r_A(E_A)$ in terms of which

$$\phi_A(E_A) = r_A(E_A)\phi(E_A). \tag{37}$$

These experiments distinguish only between a light and a heavy component. We assign atomic number 1 to the light component and 56 to the heavy one (which we call ''iron''). Here k, γ, and r_A have errors Δk, $\Delta\gamma$, and Δr_A, respectively. The equivalent nucleon flux is still given by Eq. (31), while standard propagation of errors gives, in this case,

$$\Delta\phi_{eq} = \left\{ \sum_A A^2\phi_A^2 \left(\frac{\Delta r_A}{r_A} \right)^2 + \phi_{eq}^2 \left(\frac{\Delta k}{k} \right)^2 + \left[\sum_A A\phi_A \ln(AE_N)\Delta\gamma_A \right]^2 \right\}^{1/2}. \tag{38}$$

We omit the much longer expression for $\Delta\gamma_{eq}$. For simplicity, we have neglected the error coming from the energy dependence of r_A, which we expect to be much smaller than the others. In Fig. 12 we show the equivalent nucleon flux ϕ_{eq}. It is clear from the figure that the systematic uncertainties dominate, with spreads between different experiments of up to a factor of 4.

The uncertainties in the equivalent spectral index γ_{eq} are smaller, as can be seen in Fig. 13, where only HEGRA and CASA-MIA extend to the energy region above the knee which is important to us.

We can consider, for example, an energy $E_N \simeq 10^7$ GeV, which is likely to determine the leptonic fluxes at around $E_l \simeq 10^6$ GeV, energy at which we would like to measure λ through the spectral index (we recall from GGV2 that $E_l \lesssim 0.1E_N$).

At this energy E_N, from Fig. 13, we may take half the difference between the central values of the CASA-MIA and HEGRA data as an indication of the systematic uncertainty on γ_{eq},

$$\Delta\gamma_{syst} \simeq 0.1. \tag{39}$$

Using the CASA-MIA data and the related error band, instead of the very spread HEGRA data, we can expect a reasonable statistical uncertainty

$$\Delta\gamma_{stat} \simeq 0.05. \tag{40}$$

Since α_l depends linearly on γ_{eq} and λ, the same uncertainties apply to a determination of λ. The total uncertainty in the determination of λ coming from the unknown composition of cosmic rays is now simply the sum of Eqs. (30), (39) and (40),

$$(\Delta\lambda)_{comp} \simeq (\Delta\gamma_{eq})_{comp} \simeq 0.17, \tag{41}$$

if summing the errors linearly, or

$$(\Delta\lambda)_{comp} \simeq (\Delta\gamma_{eq})_{comp} \simeq 0.11, \tag{42}$$

if we sum them in quadrature.

Finally, we can now combine all the uncertainties together to compute the overall theoretical error in the determination of λ with neutrino telescopes. From Eqs. (25), (26), (27), (30), (39), and (40) we obtain

$$\Delta\lambda \simeq 0.25 \ \ (0.21), \tag{43}$$

if summing errors linearly, or

$$\Delta\lambda \simeq 0.13 \ \ (0.11), \tag{44}$$

if summing in quadrature, where the numbers in parentheses correspond to the $\mu_F = 2m_T$ ''band'' in the charm model.

VII. CONCLUSIONS

We have examined in detail the possibility of determining the slope λ of the gluon PDF, at momentum fraction $x \lesssim 10^{-5}$, not reachable in laboratories, through the measurement in neutrino telescopes of the slope of down-going muon fluxes at $E_\mu \simeq x^{-1}$ GeV.

The method we are proposing may reasonably well reach $x \simeq 10^{-7}$, which would require 10 PeV in muon energy. At this energy, there would still be 50 events from charm if $\lambda = 0.5$ and 10 events if $\lambda = 0$. But the best measurement could be done between 100 TeV and 1 PeV of muon energy, i.e. between $x \simeq 10^{-4}$ and $x \simeq 10^{-6}$. Present data do not go below $x \simeq 10^{-5}$ and the CERN Large Hadron Collider (LHC) will not do any better. The reason is that the dominant values of x in the production of a heavy particle of mass M and rapidity y are of order $x \simeq [M\exp(\pm y)/\sqrt{s}]$ (see for example [32]) where $\sqrt{s}$ is the center-of-mass energy of the hadron

collision. Thus the smaller values of x are obtained with the smaller M and larger y for fixed $\sqrt{s}$ (14 TeV at the LHC). Even if exhaustive studies of the possible minimum x to be reached at the LHC have not yet been carried out [33], it is known that the experiments will explore the central rapidity region (the CMS and ATLAS detectors will cover $y<0.9$ only) and that bottom can be tagged, but most likely not charm[5] [34]. This means that the lowest x that LHC is expected to reach, assuming realistically that charm will not be tagged, is $x \simeq m_b \exp(-0.9)/\sqrt{s} = 1.5\times 10^{-4}$. Therefore, the method proposed here may give information on the gluon PDF at $x<10^{-5}$, a range not reachable in laboratory experiments in the near future.

To this end we studied the dependence of the leptonic fluxes and their slopes on λ. The slopes depend almost linearly on λ. We studied the uncertainties of the method we propose (excluding the experimental errors of the telescopes themselves). These come mainly from two sources: the free parameters of the NLO QCD calculation of charm production and the poorly known composition of cosmic rays at high energies.

We have seen that, for a fixed value of λ, the uncertainties give rise to an error band for the leptonic fluxes of almost one order of magnitude at the highest energies. This makes impossible a determination of λ based solely on the absolute values of the fluxes; therefore, we propose using the slopes of the fluxes. In particular we are proposing to use *down-going muons*, for energies $E_\mu \gtrsim 100$ TeV, where prompt muons dominate over conventional ones, and not up-going neutrino-induced muons whose flux is orders of magnitude smaller. While an important contribution to up-going muons is expected from astrophysical neutrinos, there is no background for down-going atmospheric muons.

The overall theoretical error, from the charm production model, on the measurement of λ, is $(\Delta\lambda)_{charm} \lesssim 0.10$. A comparable error, due to uncertainties in the cosmic ray composition, $(\Delta\lambda)_{comp} \lesssim 0.15$, must be added, so that the overall error in the determination of λ with neutrino telescopes is $\Delta\lambda \sim 0.2$.

These errors may be reduced by improving the experimental knowledge of the charm production cross sections and of the cosmic ray composition around and above the knee.

[5]Tagging is done by finding the point where the quark decays (called the vertex). The probability of decaying is exponential and higher in the region close to the collision point. The only way to tell charm from bottom is by the distance from the collision to the vertex and on average bottom mesons live longer than charmed mesons. Thus, to detect charm with a good degree of confidence, one needs to select vertices close to the collision point. But in this region the vertices from bottom decay dominate, because the number of decay channels of the b quark is 5 times larger than that of the c quark.

ACKNOWLEDGMENTS

The authors would like to thank M. Mangano, P. Nason, L. Rolandi, and D. Treleani for helpful discussions. We also thank M. Mangano and P. Nason for the MNR program. This research was supported in part by the U.S. Department of Energy under grant DE-FG03-91ER40662 Task C.

[1] T. Sjöstrand, Comput. Phys. Commun. **82**, 74 (1994).
[2] G. Gelmini, P. Gondolo, and G. Varieschi, Phys. Rev. D **61**, 036005 (2000).
[3] G. Gelmini, P. Gondolo, and G. Varieschi, Phys. Rev. D **61**, 056011 (2000).
[4] L. Pasquali, M.H. Reno, and I. Sarcevic, Phys. Rev. D **59**, 034020 (1999).
[5] M. Thunman, G. Ingelman, and P. Gondolo, Nucl. Phys. B (Proc. Suppl.) **43**, 274 (1995); P. Gondolo, G. Ingelman, and M. Thunman, *ibid.* **48**, 472 (1996); M. Thunman, Ph.D. Thesis, Uppsala University, 1996; M. Thunman, G. Ingelman, and P. Gondolo, Astropart. Phys. **5**, 309 (1996).
[6] A.H. Mueller, hep-ph/9911289.
[7] A.L. Ayala, M.B. Gay Ducati, and E.M. Levin, Phys. Lett. B **388**, 188 (1996).
[8] A.L. Ayala, M.B. Gay Ducati, and E.M. Levin, hep-ph/9608304; Nucl. Phys. **B511**, 355 (1998).
[9] M.L. Mangano, P. Nason, and G. Ridolfi, Nucl. Phys. **B373**, 295 (1992); **B405**, 507 (1993).
[10] J.C. Collins, and R.K. Ellis, Nucl. Phys. **B360**, 3 (1991); R.K. Ellis and D.A. Ross, *ibid.* **B345**, 79 (1990); S. Catani, M. Ciafaloni, and F. Hautmann, *ibid.* **B366**, 135 (1991).
[11] M.L. Mangano, Report No. CERN-TH/97-328, hep-ph/9711337.
[12] M.L. Mangano, LHC98 Workshop, CERN-TH (unpublished).
[13] CDF Collaboration, F. Abe *et al.*, Phys. Rev. Lett. **79**, 584 (1997); Phys. Rev. D **56**, 3811 (1997), and references therein.
[14] L. Durand and H. Pi, Phys. Rev. Lett. **58**, 303 (1987).
[15] D. Treleani, Int. J. Mod. Phys. A **11**, 613 (1996).
[16] D. Treleani (private communication).
[17] E769 Collaboration, G.A. Alves *et al.*, Phys. Rev. Lett. **77**, 2388 (1996).
[18] E769 Collaboration, G.A. Alves *et al.*, Phys. Rev. Lett. **77**, 2392 (1996).
[19] S. Frixione, M.L. Mangano, P. Nason, and G. Ridolfi, Report No. CERN-TH/97-16, hep-ph/9702287.
[20] A.D. Martin, R.G. Roberts, W.J. Stirling, and R.S. Thorne, Eur. Phys. J. C **4**, 463 (1998).
[21] Particle Data Group, C. Caso *et al.*, Eur. Phys. J. C **3**, 1 (1998).
[22] LEBC-EHS Collaboration, M. Aguilar-Benitez *et al.*, Z. Phys. C **40**, 321 (1988).
[23] ACCMOR Collaboration, S. Barlag *et al.*, Z. Phys. C **39**, 451 (1988).
[24] LEBC-EHS Collaboration, R. Ammar *et al.*, Phys. Rev. Lett. **61**, 2185 (1988).
[25] E653 Collaboration, K. Kodama *et al.*, Phys. Lett. B **263**, 573 (1991).

[26] A.D. Martin, R.G. Roberts, and W.J. Stirling, Phys. Lett. B **387**, 419 (1996).
[27] H.L. Lai *et al.*, Phys. Rev. D **55**, 1280 (1997).
[28] JACEE Collaboration, K. Asakimori, *et al.*, Astrophys. J. **502**, 278 (1998); UWSEA-PUB-95-07, in 24th International Cosmic Rays Conference (ICRC 95), Rome, Italy, 1995, p. 707, astro-ph/9509091.
[29] CASA-MIA Collaboration, M.A.K. Glasmacher *et al.*, Astropart. Phys. **10**, 291 (1999); Nucl. Phys. B (Proc. Suppl.) **75A**, 241 (1999).
[30] HEGRA Collaboration, F. Arqueros *et al.*, astro-ph/9908202.
[31] B. Wiebel-Sooth, P.L. Biermann, and H. Meyer, Astron. Astrophys. **330**, 389 (1998).
[32] S. Catani *et al.*, hep-ph/0005025.
[33] M. Mangano (private communication).
[34] L. Rolandi (private communication).